MODELING OF AZ80 MAGNESIUM ALLOY CASTING PROCESS UNDER DIFFERENT ELECTROMAGNETIC FREQUENCY

Yuanyuan Bai[1], Rufei Wei[2,3], Qichi Le[1*], Haitao Zhang[1]

[1] Key Laboratory of Electromagnetic Processing of Materials, Ministry of Education, Northeastern University, Shenyang, Liaoning 110004,China
[2] School of Metallurgy Engineering, Anhui University of Technology, Ma'anshan, Anhui 243002, China
[3] Key Laboratory of Metallurgical Emission Reduction & Resources Recycling, Ministry of Education, Anhui University of Technology, Ma'anshan, Anhui 243002, China

[*]corresponding author: e-mail: qichil@mail.neu.edu.com (Q. Le), byy132@hotmail.com (Y. Bai)

Resume

The paper aims to clarify the effects of electromagnetic frequency on magnesium alloy AZ80 billets during low frequency electromagnetic casting. It proposes a mathematic model, verified against the temperature measurements obtained from AZ80 alloy billet of 160 mm in diameter, to predict the interaction of electromagnetic field, fluid flow, and temperature distribution. The sump depth becomes deeper and the maximum sustained speed of melt flow increases with the increase of electromagnetic frequency. By the analysis of the effects of fluid flow and temperature field on the solidification in the presence of electromagnetic field, the best electromagnetic parameters are given.

Available online: http://fstroj.uniza.sk/journal-mi/PDF/2016/19-2016.pdf

Article info

Article history:
Received 22 August 2016
Accepted 12 December 2016
Online 04 February 2017

Keywords:
Low frequency electromagnetic casting;
Magnesium alloy;
Temperature field;
Fluid flow.

ISSN 1335-0803 (print version)
ISSN 1338-6174 (online version)

1. Introduction

Compared with steel and aluminum, magnesium (Mg) is used commonly as the lightest structural metal for the low specific gravity. Additionally, there are many other advantages of magnesium, such as high specific strength and specific stiffness, excellent damping capacity and recyclability, relatively good conductivity and shielding capacity, and etc. The magnesium alloy has a great potential to be used in automobile, electronic products, aerospace and defense. And the application of magnesium alloys grows at the fastest rate every year in the world [1 - 4]. The research of magnesium alloys has been more extensive since 2000. AZ80 alloy is one of the most typical cast Mg alloys with low price and good mechanical properties [5 - 8]. There have been several studies to investigate AZ80 magnesium alloy. Hilpert et al. [9] studied corrosion fatigue behavior of the high-strength magnesium alloy AZ80 and showed that roller burnishing led to outstanding fatigue performance. In another study, effect of heat treatment on microstructure and tensile deformation of Mg AZ80 alloy at room temperature has been investigated. It has been shown that the dissolution of γ-phase in materials homogenized for 5 h significantly improves the casting‘s ductility [10]. Moreover, it has also been reported that continuous networks of β-Mg17Al12 formed along grain boundaries acted as effective crack propagation paths, which had negative effects on the weld strength [11].

Up to now, most of the magnesium alloy products are fabricated by direct chill (DC) casting. It is very easy to process foundry defects, especially hot cracking appearing in DC casting when filling of the mould cavity, because heat transfer, which takes place between the metal surface and the walls of the mould, will directly affect the subsequent processing as genetic effect. Therefore, it is important to eliminate the casting defects in order to improve microstructure and properties of the alloy. Low-frequency electromagnetic casting (LFEC) is developed by Cui and his colleagues [12 - 15], which can improve properties of the alloy by precisely controlling the fluid flow and temperature field. Their research suggests the application of low-frequency electromagnetic field can refine microstructure of aluminum alloys remarkably, decrease the macro segregation, increase the mechanical properties of casting alloys, and improve the surface quality of ingot and hinder crack efficiently.

In addition, with the development of finite element calculation, numerical simulation has become the effective and convenient technology tools of engineering analysis science research besides experiment and theory. A large number of experiments were performed to obtain best process parameters, but this resulted in costly and time consuming and sometimes it was impossible in the past. Thus, the process was modeled and analyzed by the finite element method at first, and then the result was verified by experiments. Many mathematical models for a continuous casting process have been developed. There are also some studies about semi-continuous casting process simulation when the low-frequency electromagnetic exists. Zhang et al. [16, 17] presented a numerical simulation model for 7XXX aluminum alloys which could predict electromagnetic field, fluid flow, heat transfer and solidification during low frequency electromagnetic casting. Yoshioka et al. [18] studied the heat transfer and solidification processes of alloy melt with undercooling. In this investigation, an analytical model was proposed to predict the temperature change, interface movement, and solute concentration distribution during the solidification of an undercooled Bi–Sn melt. Faraji et al. [19] investigated the finite element method (FEM) and an experiment of the accumulative back extrusion (ABE) processing of an AZ91 magnesium alloy. Le et al. [20] studied the effect of electromagnetic field on the hot-top casting by numerical simulation. Kageyama et al. [21] developed a three dimensional numerical model and predicted the behavior of steel in the field of an electromagnetic caster. Bermudez et al.[22]studied the ingot temperature in DC and EMC metal castings, and they solved the free boundary problem using a fixed domain method. Shao et al. [23] investigated the influence of low frequency electromagnetic field and power ultrasonic field on DC casting. However, there are few reports that discuss the effects of low-frequency electromagnetic field on AZ80 magnesium alloy systematically during DC casting with the mold of forged aluminum by numerical calculation.

In this paper, the FEM and an experimental investigation were performed to investigate the effects of the electromagnetic field on the semi continuous casting of AZ80 magnesium alloy. This developed model includes non-linear material properties of specific heat and thermal conductivity as well as phase changes during solidification.

2. Numerical simulations

Many facts influenced the flow and heat transfer of melt, in order to solve the problem, the model were simplified and some necessary assumptions were given:

(1) The meniscus shape and calculation of the solute field were not comprised in the study.

(2) The molten magnesium alloys deemed as an incompressible fluid, so the density of the melt was set down as constant.

(3) The effect of displacement current was ignored. Because the molten metal is good conductor of electricity in which the charge relaxation time is much lower than the transit time of electromagnetic waves.

(4) The distribution of the magnetic field was not influenced by the variety of the fluid field. As for LFEC process of magnesium alloys, the magnetic Reynolds number R_m is less than 1 (where μ is permeability, σ the electric conductivity, U_0 the characteristic velocity and L_0 is characteristic length), which will result the second term of right hand side of the Ohm's Law (J=σ(E+U×B)) is ignored.

(5) Joule heating was not considered in this model because it was so tiny compared with the total quantity of heat in the system. Compared to the entropy inflow with the liquid magnesium, the Joule heat produced during LFEC process is so small that can be ignored.

The governing equations in calculation of LFEC process are expressed as follows [17]:

Ampere's law:

$$\nabla \times \mathrm{E} = -\frac{\partial B}{\partial t} \tag{1}$$

Faraday's law:

$$\nabla \times \mathrm{B} = \sigma \mathrm{E} \tag{2}$$

Gauss's law of electric field:

$$\nabla \cdot \mathrm{E} = 0 \tag{3}$$

Gauss's law of magnetic field:

$$\nabla \cdot \mathrm{B} = 0 \tag{4}$$

where E is the electric field intensity vector, B is the magnetic flux density vector; t is the time and s the electric conductivity.

It is essential to give a constitutive equation about electromagnetic volume density f_{em}, which can be given as:

$$f_{em} = J \times B \tag{5}$$

On the basis of hypothesis (4), the conduction current J can be expressed as:

$$J = \sigma E \tag{6}$$

The time average electromagnetic volume force density F which is introduced to link electromagnetic field and other physics fields can be obtained as:

$$\mathrm{F} = \frac{1}{2} R_e (J \times B) \tag{7}$$

where, R_e is the real part of a complex quantity.

Computer simulations of the effects of various casting conditions on the steady-state temperature distribution and sump profile and flow patterns during LEFC process of AZ80 alloy are performed with ANSYS software. To analyze the problem, 2-Dimensional models are constructed in ANSYS finite element software. Considering the symmetry, only one half of the billet is modeled. The calculation domain 1600 mm high and 80 mm in radius is divided into rectangular blocks. Thermophysical parameters used in these simulations are described in Fig. 1. The boundary conditions at the inlet and outlet are a constant temperature and a constant velocity. All free surfaces are treated as the static adiabatic wall. Symmetry axis boundary condition is applied to axisymmetric boundary condition. Mold cooling refers to the region where the billet is within the mold at a given time. Equation (8) and (9) expresses these boundary conditions:

$$k_{thermal} \frac{\partial T}{\partial n} = h(T - T_{en}) \tag{8}$$

$$h = h_{contact}(1 - f_s) + h_{air} \times f_s \tag{9}$$

where h is the heat transfer coefficient at the boundary; T_{en} is the environment temperature and it is set to 323 K; $h_{contact}$ is the heat transfer coefficient at the mold and is given as 1000 W $m^{-2}K^{-1}$; h_{air} is the heat

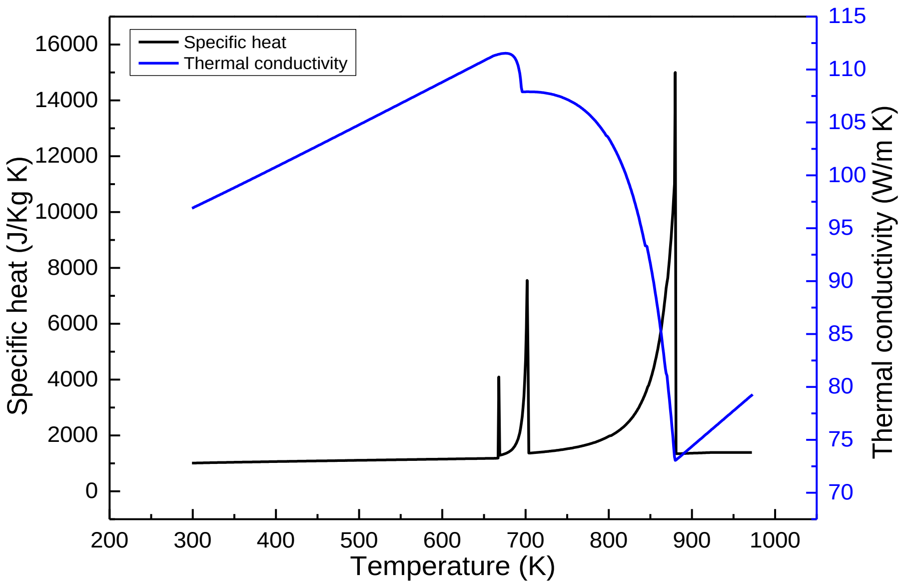

Fig. 1. The values of specific heat and thermal conductivity.
(full colour version available online)

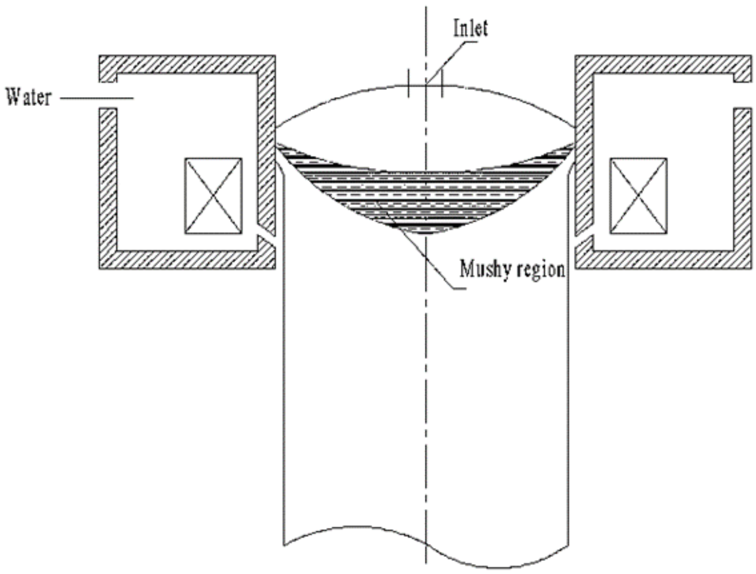

Fig. 2. Schematic diagram of LFEC process of AZ80 Mg alloy billets

is comprised of two regions: the impingement zone and the free falling zone, which refer to the areas below the mold that are in contact with water. The idealized boiling water curves describe the relationships to the heat transfer coefficient during secondary cooling [24]. This boundary condition is treated as the moving wall, and its velocity is 0.00133 m.s^{-1}. In addition, the environment temperature is given as 300 K. Calculations are stopped as soon as the steady state is achieved.

3. Experimental procedures

The material used in this study was an as-cast AZ80 magnesium alloy with a main composition of Al 7.9 – 9.2, Zn 0.7 – 0.8, Mn 0.12 – 0.15, and Mg balance. High purity Mg, Al, and Zn were used to prepare the alloys, Mn was added in the form of Al-9 wt. % Mn master alloy, respectively. The melting experiment of alloy was conducted by a self-developed resistance furnace under the No. 2 covering flux and CO_2 + 0.5 vol. % SF6 atmosphere, which was to protect molten magnesium from oxidation (Fig. 2).

Since the liquidus temperature of the alloy was 880 K, the melt was overheated to 930 ± 5 K; this temperature had been verified to maintain the alloy composition as its initial ingredient. The metal was held for 20 min to ensure the alloying elements were completely dissolved and a homogenous composition was obtained. The melt was poured to a water-cooled mold with a diameter of 160 mm, a height of 120 mm and a wall-thickness of 10 mm at 930 K and cast into billets with a diameter of 160 mm at a velocity of 0.00133 $m.s^{-1}$. The cooling water flow rate was 70 $L.min^{-1}$ during the casting. The electromagnetic field was applied by a 100 turns water-cooling copper coil surrounding the mold made of forged aluminum. The experiment of LFEC results was compared with the simulation results. The cooling curves of different positions of the LFEC ingots were measured by means of five K-type chromel-alumel thermocouple, which were even distribution of radial direction of billet.

4. Results and discussions

4.1 Comparison between calculated results and experimental results

Fig. 3 shows the comparison of between the calculated results and the measured results for cooling curves at distance of 0, 0.04 and 0.08 m from the center of the billets during the LFEC process. It is found that numerical simulation results are basically consistent with the experiment results and the model is effective and feasible. First, the temperature of melt slow descends to liquidus due to the conduction of the mould and cooling water, and then the temperature continues to decrease at a higher rate but the cooling rate of measured positions are totally different. Additionally, the cooling rate in the edge position of billet is significant higher than other position because there is a larger thermal conductivity rate at the region closed to the mould.

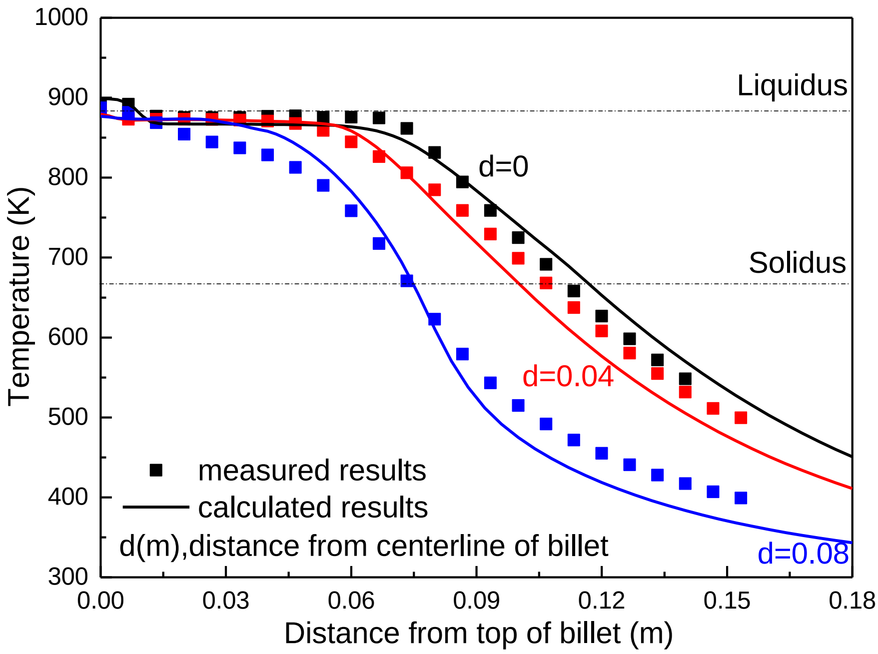

Fig. 3. Comparison between the calculated and measured results: the cooling curves in LFEC processing.

(full colour version available online)

In order to investigate the effects of electromagnetic parameters on distribution of temperature field, fluid flow and heat transfer, all parameters except electromagnetic frequency and intensity are fixed. In the first place the effect of frequency is mainly analyzed, therefore, the electromagnetic intensity keeps being 6000At, and electromagnetic frequency is set as 10 Hz, 20 Hz, 30 Hz, 50 Hz and 100 Hz, respectively. In the second place, the electromagnetic frequency keeps being 30 Hz, and electromagnetic intensity is set as 6000 At, 9000 At, 12000 At, respectively.

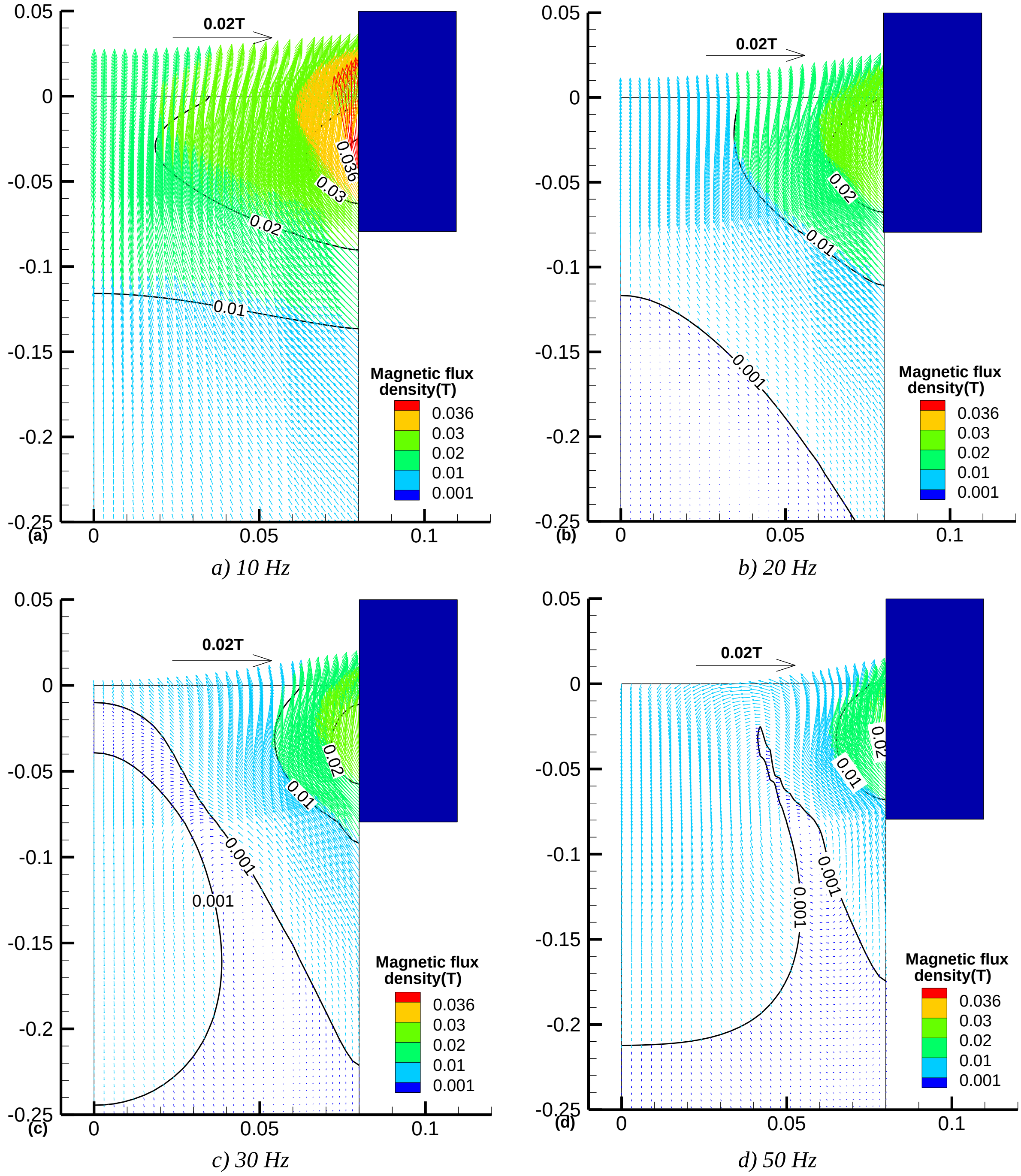

Fig.4. Magnetic flux density contours and vectors under different electromagnetic frequency.

(full colour version available online)

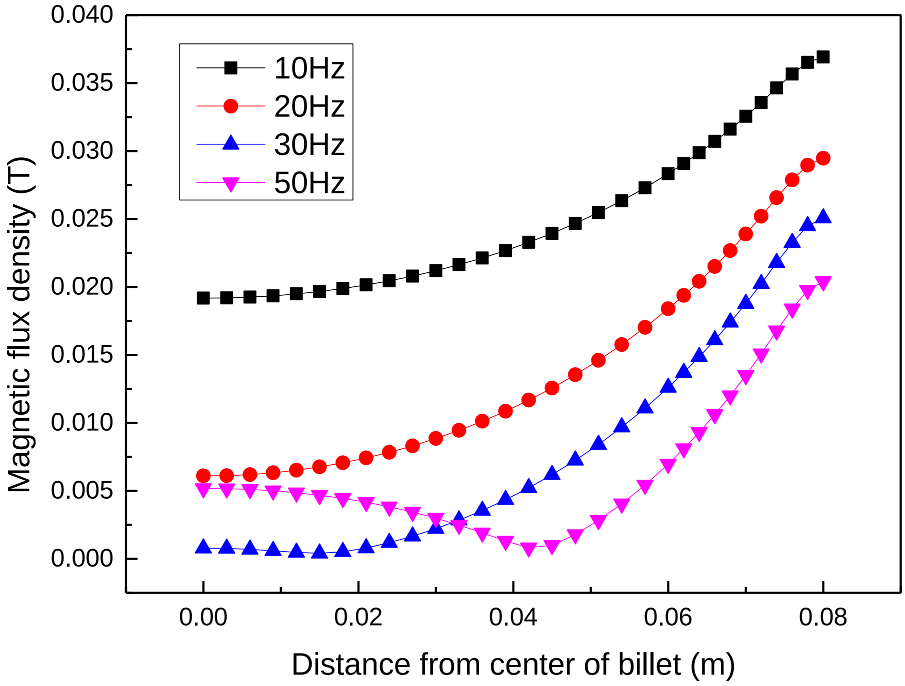

Fig.5. Magnetic flux density from the surface to the center of the billets on the given path (y = -0.035 in Fig.4) under different electromagnetic frequency.

(full colour version available online)

4.2 Magnetic flux density

The magnetic flux density contours and vectors in the billets cast during the LFEC process at various electromagnetic frequency are shown in Fig. 4. It is found that the maximum of magnetic flux density decrease slowly with the increase of electromagnetic frequency. Due to the skin effect of alternative electromagnetic field, the magnetic flux density declines from the surface to the center of billet, when the frequency is lower level (10 Hz and 20 Hz). Additionally, there is a vortex ofmagnetic flux density in the billets when the frequency is over 30 Hz. Fig. 5 shows variation of magnetic flux density on given path (y = -0.035 in Fig. 4) from the center of billets to the outer surface of the mold under different electromagnetic frequency. The distribution of electromagnetic wave in conductor can be expressed as equation (10):

$$B = B_0 e^{-r\sqrt{\pi f \mu \sigma}} \qquad (10)$$

where r is the distance from the surface to the center of billets along the given path, f the frequency and B_0 is the magnetic flux density at the surface of billets along the given path. From this we could know the magnetic flux density decreases exponentially from surface to the center of billet, and the attenuation rate increases with increasing frequency. Nevertheless, the magnetic flux density decreases first and then increases when the frequency exceed 30 Hz, and there is a trend to the surface of billet on the location of the minimum of the magnetic flux density as seen in Fig. 5. The main reason is that the eddy current introduced by the source current in the coil, which is opposite to the source current. The electromagnetic field of same frequency generated by the eddy current also is opposite to the electromagnetic field generated by the source current. The magnetic flux density showed in Fig. 4 is the superimposed result of the two electromagnetic fields mentioned above. The penetrating depth of electromagnetic field produced by the source current is larger than the eddy current when the frequency is low. Therefore, the magnetic flux density attenuates exponentially from surface to the center of billet under frequency of 10 Hz, 20 Hz and 30 Hz. However, the penetrating depth electromagnetic field produced by the source current is shallower than that by the eddy current in the center zone of billets when the frequency is greater than 30 Hz, which results in the varying of magnetic flux density in the center of billets.

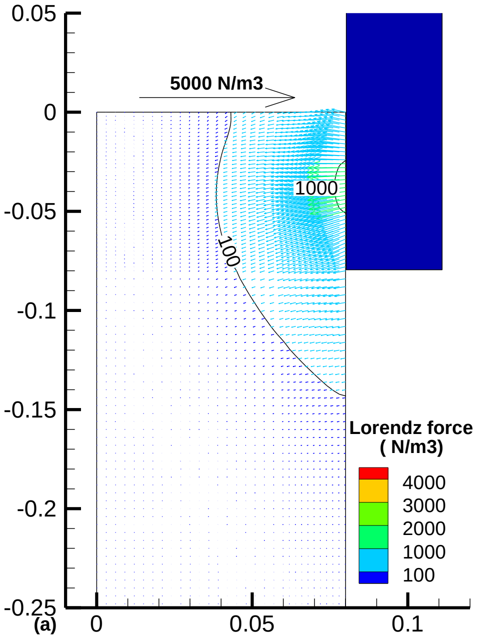

a) 10 Hz

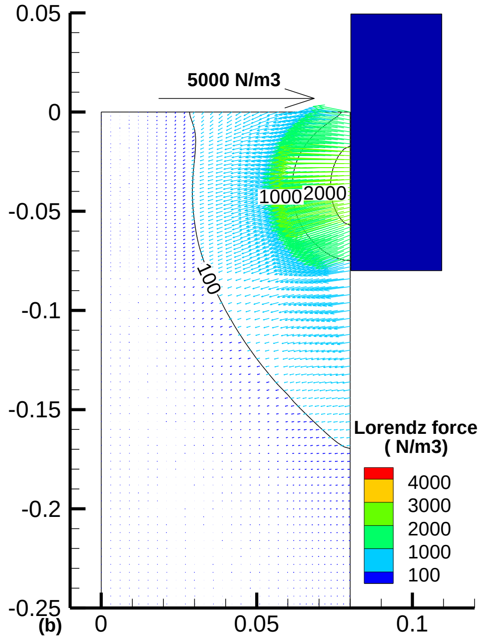

b) 20 Hz

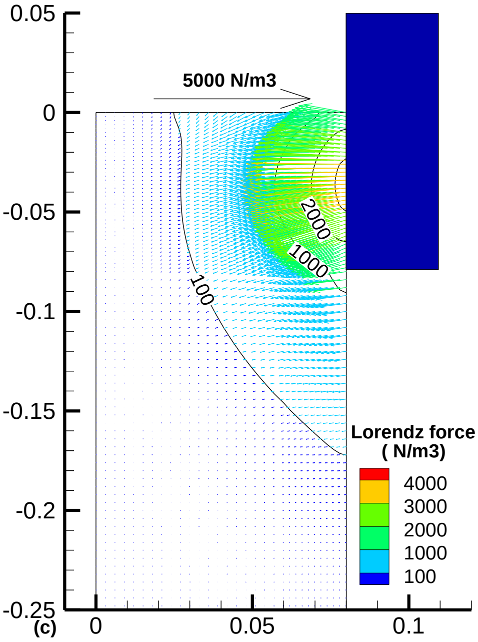

c) 30 Hz

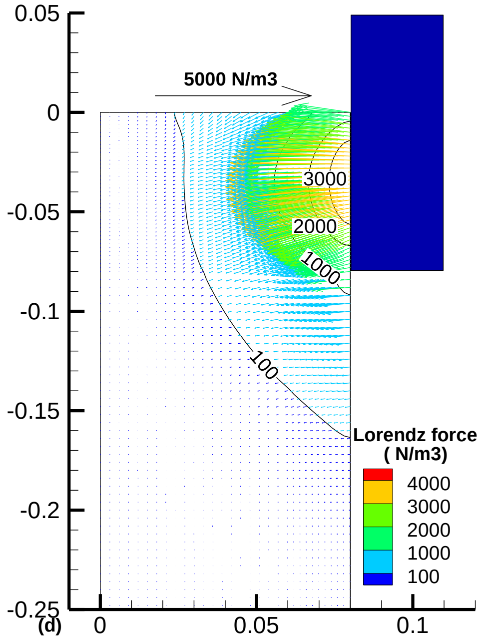

d) 50 Hz

Fig.6. Time average electromagnetic volume force density contours and vectors under different electromagnetic frequency.

(full colour version available online)

4.3 Time average electromagnetic volume force density

Fig. 6 shows the time average electromagnetic volume force density contours and vectors when electromagnetic frequency is in the range of 10 – 5 0Hz. It is found that the time average electromagnetic volume force density in the area of skin effect increases when electromagnetic frequency increase. In addition, the increase of frequency has no effect on the direction of the electromagnetic volume force density. The time average electromagnetic volume force from the surface to the center of the billets on the given path (y = -0.035 in Fig. 4) under different electromagnetic frequency are shown in Fig. 7. The direction of the electromagnetic volume force density on the path is perpendicular to the surface and pointing to the center of billets. According to reference [16],

$$F = F_0 e^{-2r\sqrt{\pi f \mu \sigma}} \tag{11}$$

where F_0 is the electromagnetic volume force density at the surface of billets along the given path. In the light of Eq. (11), like the magnetic flux density, the electromagnetic volume force density decreases exponentially from surface to the center of billet, and the attenuation rate increases with increasing frequency, as seen in Fig. 7.

4.4 Fluid flow field

Figs. 8 - 10 show velocity vectors, velocity profiles and streamline patterns under different electromagnetic frequency. The melt flow is similar for all four different cases. The direction of melt flow is not changed with electromagnetic frequency as seen in Fig. 8. It is, however, clearly seen that the maximum velocity of melt flow increases with increasing electromagnetic frequency in Fig. 9, which is same with the change trend of electromagnetic volume force. In addition, it is observed that there is a lager eddy current in molten pool and a small circulation near the solidification front at the surface region of the billet from Fig. 9. Moreover the location of maximum velocity is near the surface of billet, and the location of minimum velocity

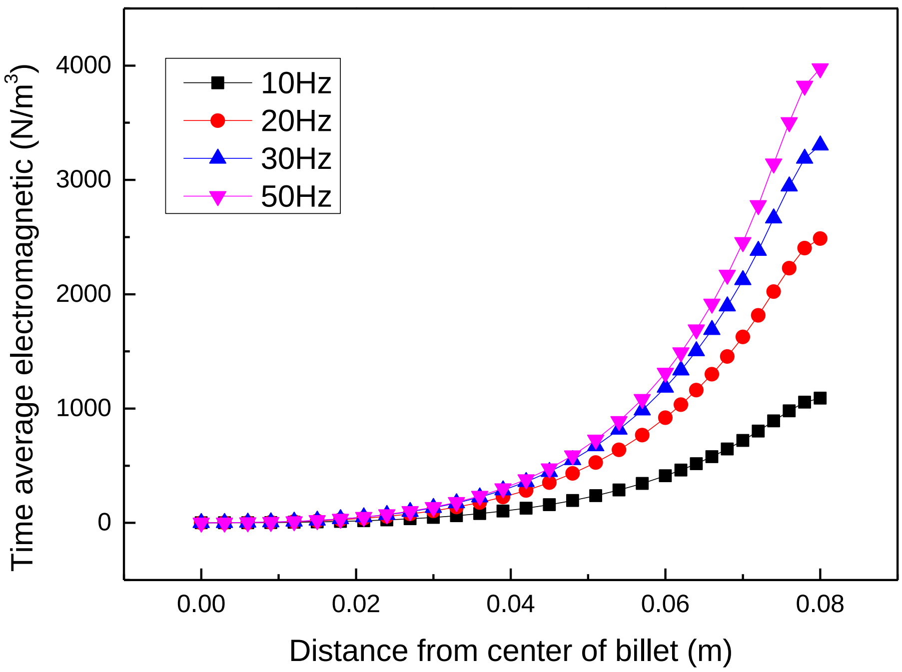

Fig.7. Time average electromagnetic volume force from the surface to the center of the billets on the given path(y=-0.035in Fig.4) under different electromagnetic frequency.
(full colour version available online)

is the inlet. The location of maximum velocity moves to the center of billet with the increase of electromagnetic frequency. The velocity distribution is non-uniform in the given path when the electromagnetic frequency is 10 Hz. As shown in Fig. 11, the velocity is quite well-distributed when electromagnetic frequency is in the range of 20 – 50 Hz. It is reason that zone of electromagnetic volume force reduces when electromagnetic frequency increases, caused by the electromagnetic penetration depth decreases with the increase of electromagnetic frequency. It means that the non-evenness of flow due to the skin effect of alternative electromagnetic field.

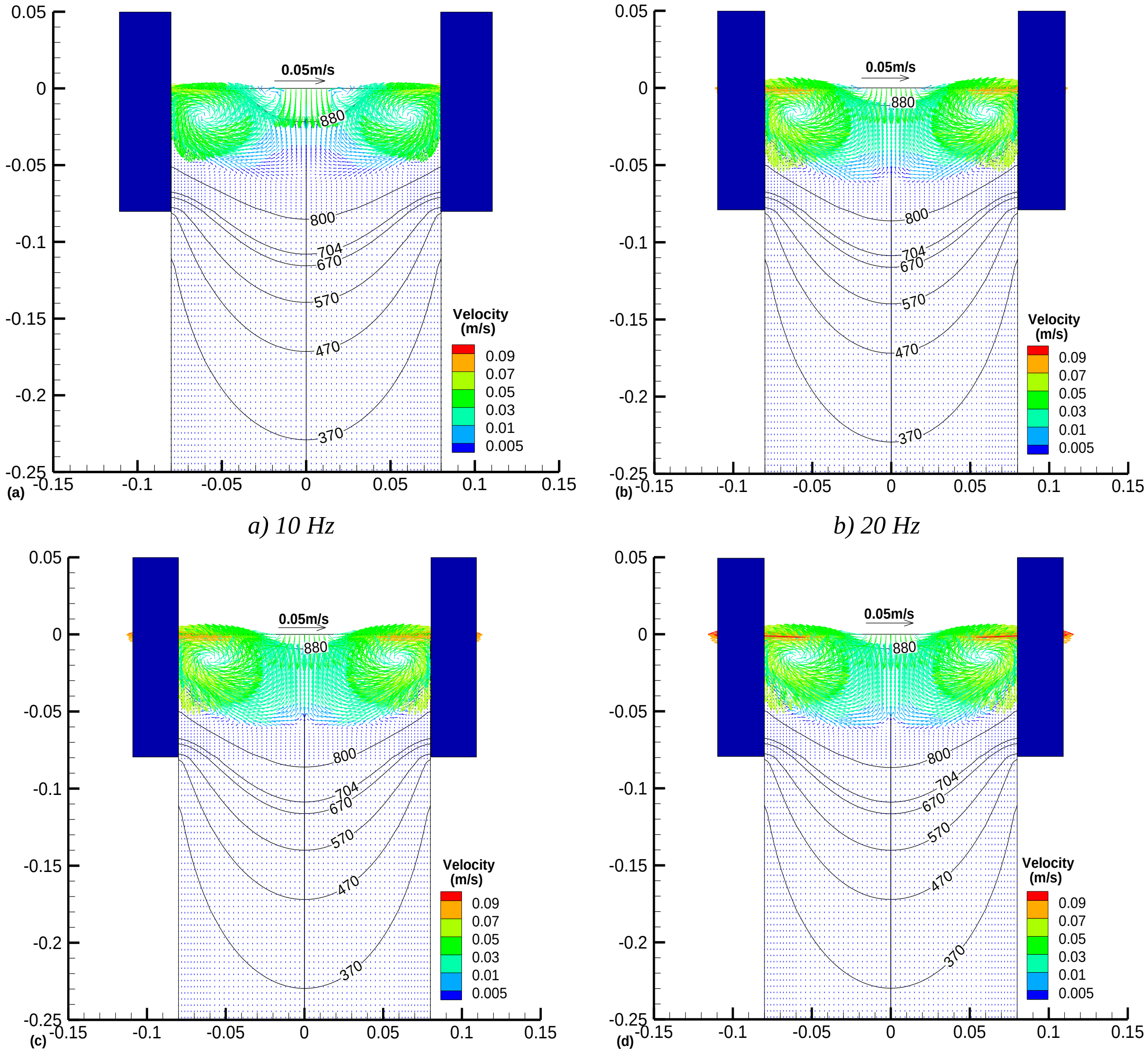

a) 10 Hz *b) 20 Hz*

c) 30 Hz *d) 50 Hz*

Fig.8. Velocity vectors with temperature profiles under different electromagnetic frequency.

(full colour version available online)

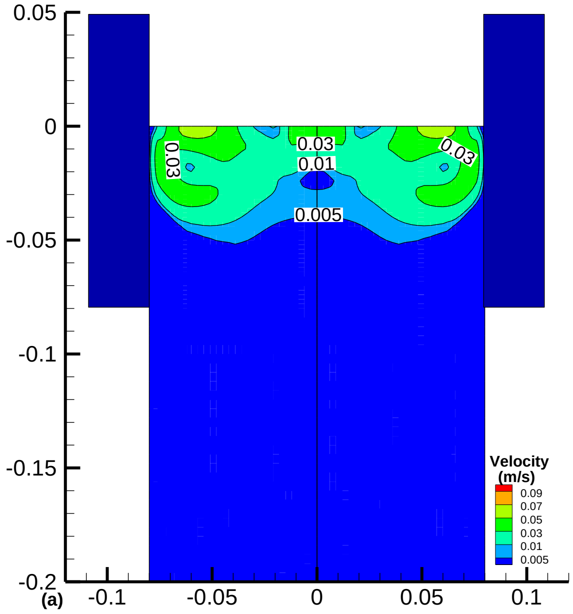

a) 10 Hz

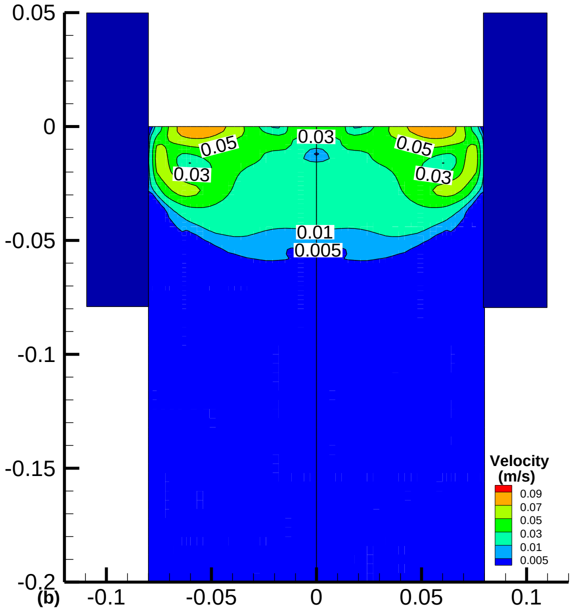

b) 20 Hz

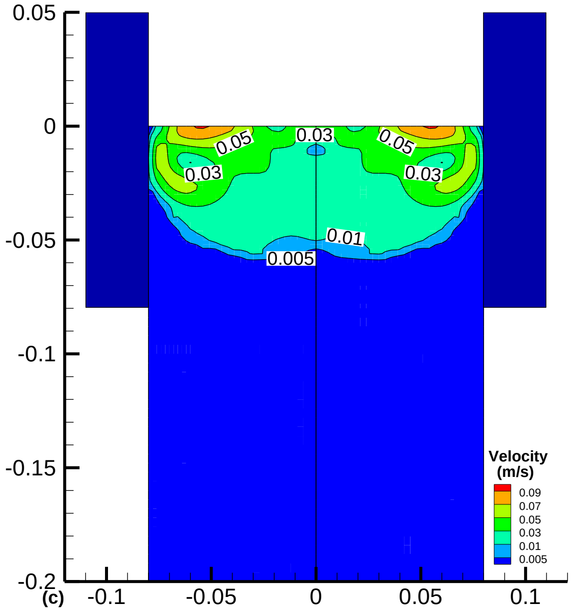

c) 30 Hz

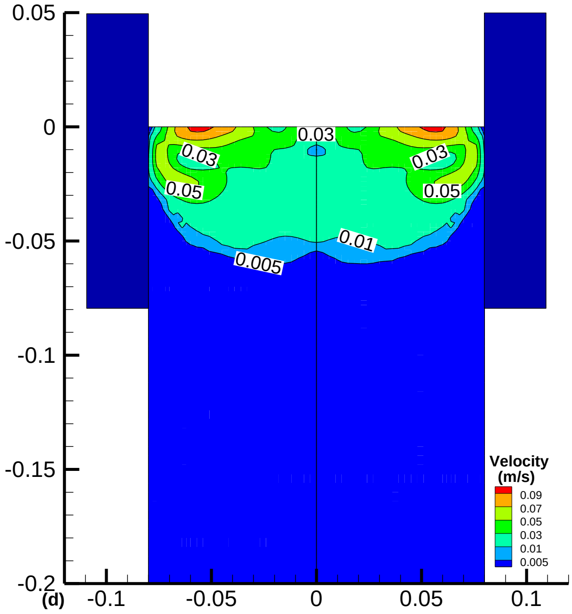

d) 50 Hz

Fig.9. Velocity profiles under different electromagnetic frequency.

(full colour version available online)

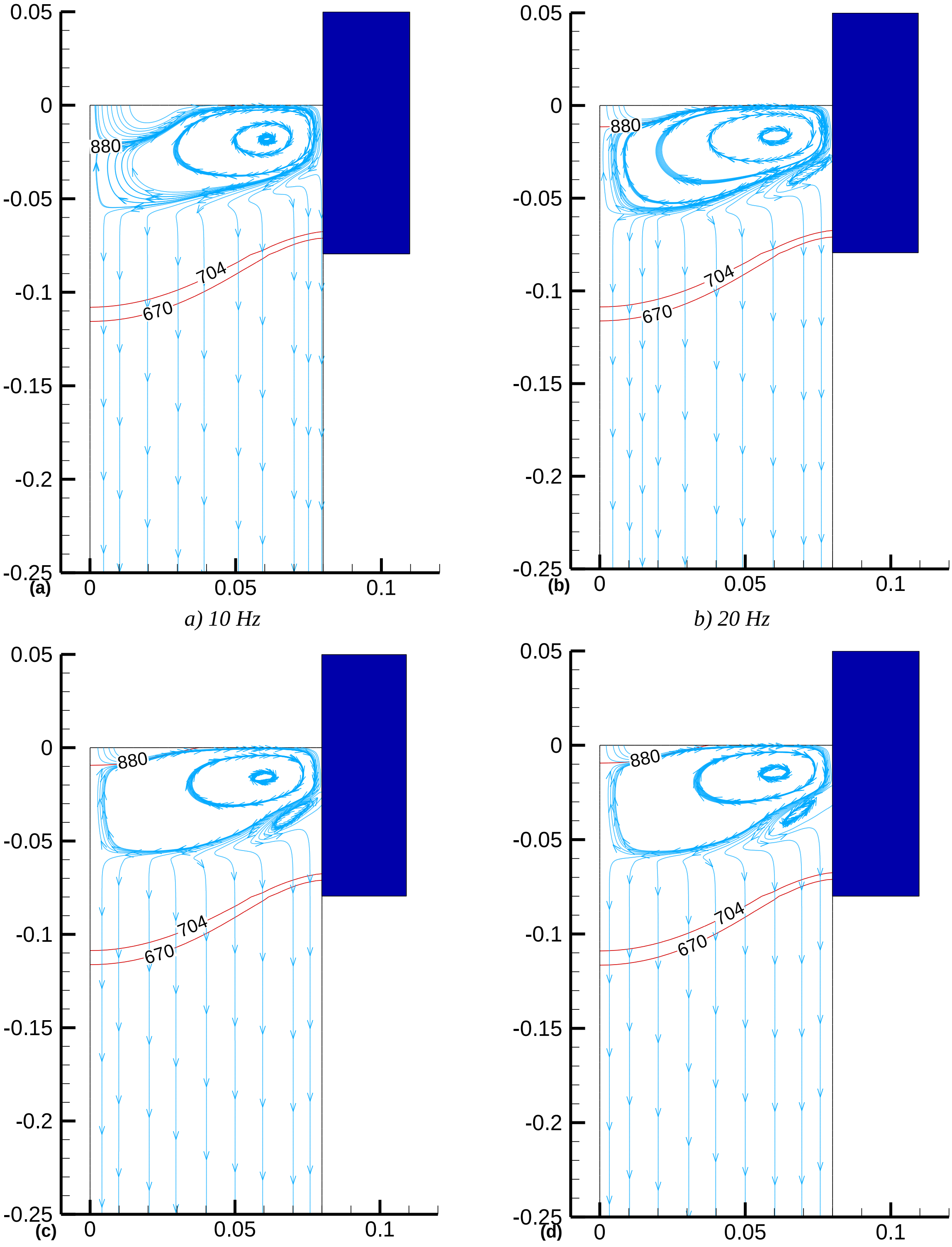

a) 10 Hz b) 20 Hz c) 30 Hz d) 50 Hz

Fig.10. Streamline patterns with temperature profiles under different electromagnetic frequency.

(full colour version available online)

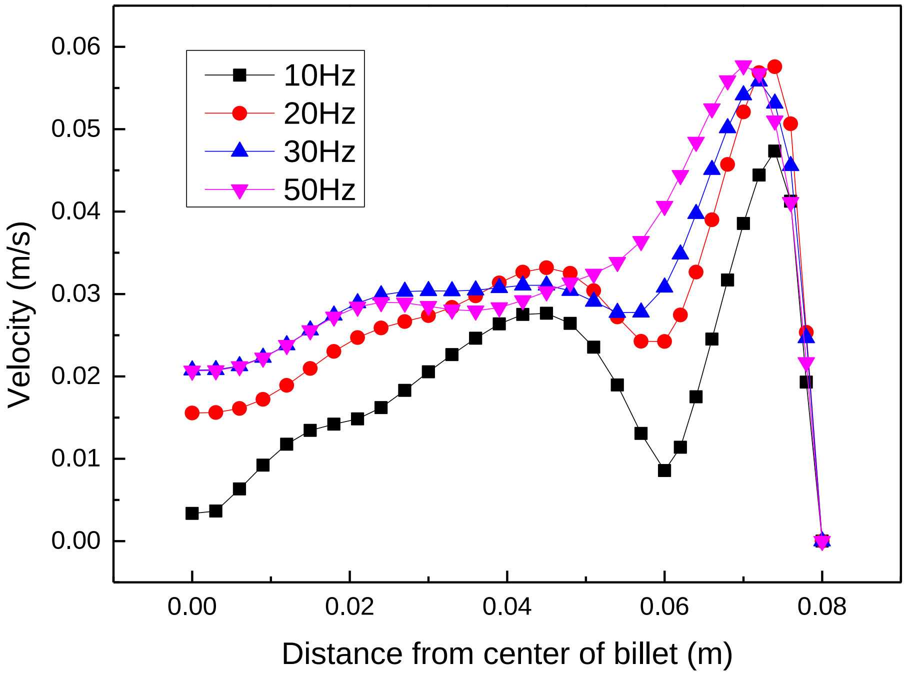

Fig.11.Velocity on the given path(y=-0.02 in Fig.4) under different electromagnetic frequency.
(full colour version available online)

4.5 Temperature field

The temperature profiles under different electromagnetic frequency are shown in Fig. 12. It is found that the uniform temperature distribution is obtained under the function of electromagnetic field. However, the temperature field is influenced little by the electromagnetic frequency. Fig. 13 shows the sump shape and sump depth under different electromagnetic frequency. It is observed that electromagnetic frequency has no effect on the sump shape, and the sump depth becomes deeper with the increase of electromagnetic frequency, but it shows a little drop as the frequency is 30 Hz. This is because the increase of intensity determined by the electromagnetic volume force.

5. Conclusions

In this study, the effects of electromagnetic frequency on AZ80 alloys during DC casting process are investigated. The study has focused on the influence of electromagnetic field on the magnetic flux density, time average electromagnetic volume force density, flow field and temperature field. The model could be used to predict the optimum process parameters on electromagnetic frequency and electromagnetic intensity.

Increasing the electromagnetic frequency leads to a decrease in magnetic flux density, an increase in electromagnetic force, first rise and then descending in relative velocity, and tiny changes in temperature field. The uniform temperature field can be obtained by electromagnetic frequency more than 30 Hz.

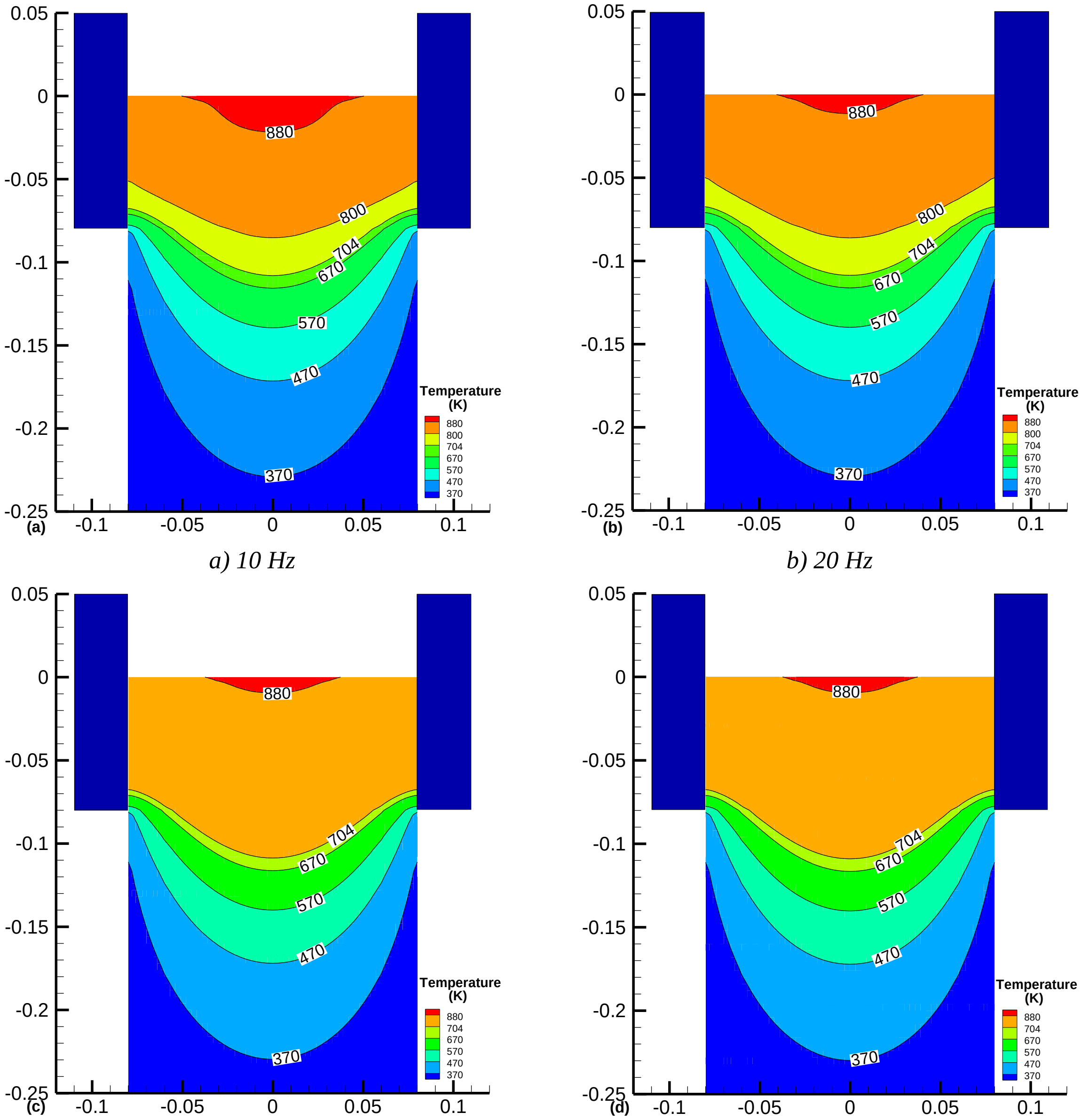

a) 10 Hz *b) 20 Hz*

c) 30 Hz *d) 50 Hz*

Fig.12. Temperature profiles under different electromagnetic frequency.

(full colour version available online)

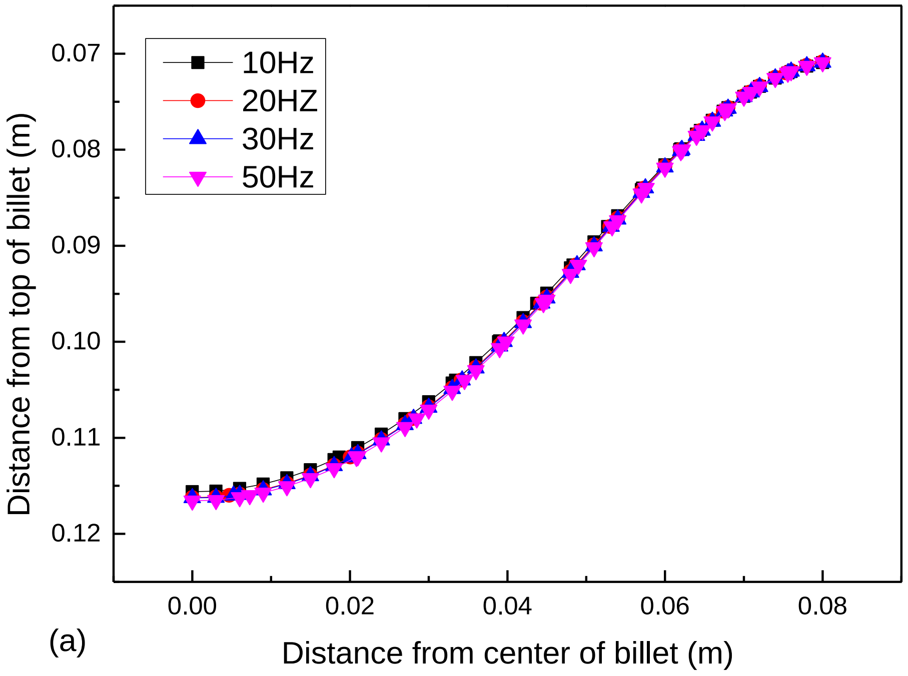

a) on sump shape

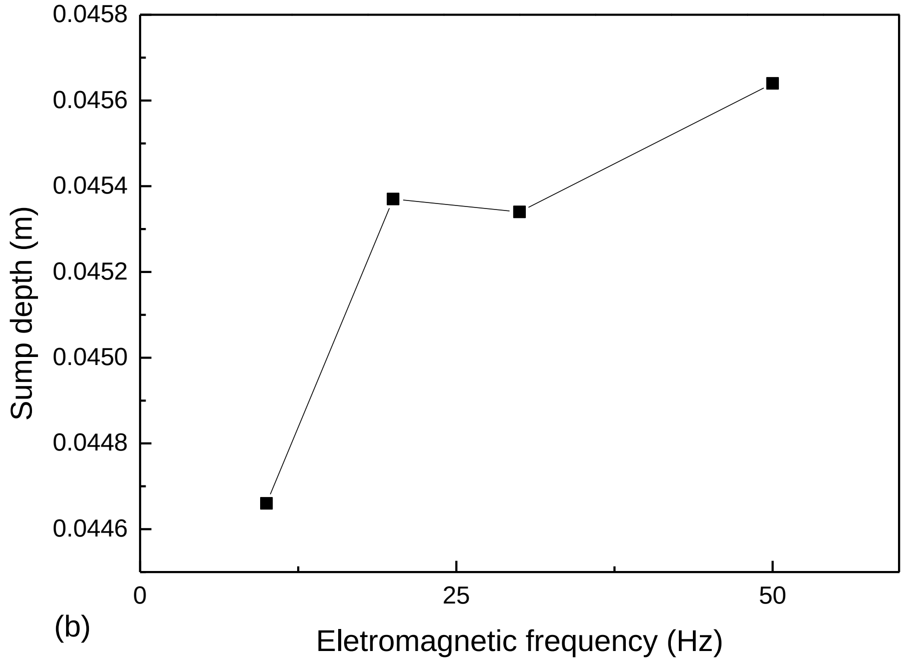

b) on sump depth

Fig. 13. The effect of electromagnetic frequency.

(full collour version available online)

Acknowledgement

This research was financially supported by the Major State Basic Research Development Program of China (Grant No. 2013CB632203), the National Basic Research Program of China (Grant number 2012CB723307-03) and the National Key Research and Development Program of China (Grant No. 2016YFB0301104)

References

[1] F. Fereshteh-Saniee, K. Fallah-Nejad, A. S. Beheshtiha, H. Badnava : Materials and Design 50 (2013) 702-712.

[2] M. Li, T. Tamura, K. Miwa: Acta Materialia 55(14) (2007) 4635-4643.

[3] B. L. Mordike, T. Ebert: Mater. Sci. Eng. A 302(1) (2001) 37-45.

[4] W. Xiao, M. A. Easton, S. Zhu, M.S. Dargusch, M. A. Gibson, S. Jia, J. Nie: Adv. Eng. Mater. 14(1-2) (2012) 68-76.

[5] S. Barbagallo, H. Laukli, O. Lohne, E. Cerri: J. Alloys Compd. 378(1) (2004) 226-232.

[6] Y. Uematsu, K. Tokaji, M. Kamakura, K. Uchida, H. Shibata, N. Bekku: Mater.Sci. Eng. A 434(1) (2006) 131-140.

[7] Z. Wang, Y. Yang, B. Li, Y. Zhang, Z. Zhang: Mater. Sci. Eng. A 582 (2013) 36-40.

[8] N. Kashefi and R. Mahmudi: Materials & Design 39 (2012) 200-210.

[9] M. Hilpert, L. Wagner: J. Mat. Eng. Perform. 9(4) (2000) 402-407.

[10] I. Yakubtsov, B. Diak, C. Sager, B. Bhattacharya, W. MacDonald, M. Niewczas: Mater. Sci. Eng. A 496(1) (2008) 247-255.

[11] S. T. Niknejad, L. Liu, T. Nguyen, M.-Y. Lee, S. Esmaeili, N.Y. Zhou: Metallurgical and Materials Transactions A (2013) 1-10.

[12] J. Dong, Z. Zhao, J. Cui, F. Yu, C. Ban, Metallurgical and Materials Transactions A 35(8) (2007) 2487-2494.

[13] B. Zhang, J. Cui, G. Lu: Materials Letters 57(11) (2003) 1707-1711.

[14] B. Zhang, J. Cui, and G. Lu: Mater. Sci. Eng. A 355(1) (2003) 325-330.

[15] Y. Zuo, J. Cui, Z. Zhao, H. Zhang, L. Li, Q. Zhu: J. Mater. Sci.. 47(14) (2012) 5501-5508.

[16] H. Zhang, H. Nagaumi, and J. Cui: Mater. Sci. Eng. A 448(1-2) (2007) 177-188.

[17] H. Zhang, H. Nagaumi, Y. Zuo, and J. Cui: Mater. Sci. Eng. A 448(1-2) (2007) 189-203.

[18] H. Yoshioka, Y. Tada, K. Kunimine, T. Furuichi, and Y. Hayashi: Acta Materialia 54(3) (2006) 765-771.

[19] M. Mohamadzadeh, A. Rostampour Haftkhani, G. Ebrahimi, and H. Yoshihara: Materials & Design 35 (2012) 404-413.

[20] Q.-C. Le, S.-J. Guo, Z.-H. Zhao, J.-Z. Cui, X.-J. Zhang: J. Mater. Process. Tech. 183(2-3) (2007) 194-201.

[21] R. Kageyama: Isij International 42(2) (2002) 163-170.

[22] A. Bermúdez, M. Otero: Finite Elem. Anal. Des. 40(13) (2004) 1885-1906.

[23] Z. Shao, Q. Le, Z. Zhang, J. Cui: Materials & Design 32(8-9) (2011) 4216-4224.

[24] H. Hao, D. Maijer, M. Wells, S. Cockcroft, D. Sediako, S. Hibbins: Metallurgical and Materials Transactions A 35(12) (2004) 3843-3854.